SEMICONDUCTORS

2016 © The Authors, some rights reserved; exclusive licensee American Association for the Advancement of Science. Distributed under a Creative Commons Attribution NonCommercial License 4.0 (CC BY-NC).
10.1126/sciadv.1600076

Remarkable enhancement of charge carrier mobility of conjugated polymer field-effect transistors upon incorporating an ionic additive

Hewei Luo,[1]* Chenmin Yu,[1]* Zitong Liu,[1]† Guanxin Zhang,[1] Hua Geng,[1] Yuanping Yi,[1] Katharina Broch,[2] Yuanyuan Hu,[2] Aditya Sadhanala,[2] Lang Jiang,[2] Penglin Qi,[1] Zhengxu Cai,[1] Henning Sirringhaus,[2†] Deqing Zhang[1†]

Organic semiconductors with high charge carrier mobilities are crucial for flexible electronic applications. Apart from designing new conjugated frameworks, different strategies have been explored to increase charge carrier mobilities. We report a new and simple approach to enhancing the charge carrier mobility of DPP-thieno [3,2-*b*]thiophene–conjugated polymer by incorporating an ionic additive, tetramethylammonium iodide, without extra treatments into the polymer. The resulting thin films exhibit a very high hole mobility, which is higher by a factor of 24 than that of thin films without the ionic additive under the same conditions. On the basis of spectroscopic grazing incidence wide-angle x-ray scattering and atomic force microscopy studies as well as theoretical calculations, the remarkable enhancement of charge mobility upon addition of tetramethylammonium iodide is attributed primarily to an inhibition of the torsion of the alkyl side chains by the presence of the ionic species, facilitating a more ordered lamellar packing of the alkyl side chains and interchain π-π interactions.

INTRODUCTION

Organic semiconductors based on small conjugated molecules and polymers have received increasing attention in recent years because of their promising applications in various devices, including organic field-effect transistors (OFETs) (*1*–*10*), organic photovoltaics (OPVs) (*11*–*17*), and organic light-emitting diodes (OLEDs) (*18*, *19*). Among them, OFETs are emerging as a promising technology for the low-cost production of flexible, light-weight, ubiquitous electronic devices for the Internet of Things or wearable electronic applications (*20*, *21*). The key performance metric of OFETs is the high charge carrier mobility. One of the main factors governing charge mobilities is the chemical structure of the conjugated frameworks and the intermolecular (or interchain) π-orbital overlap (*22*, *23*). Both molecular orbital tuning and crystal engineering strategies have been intensively explored to enhance charge mobilities of small molecular semiconductors, and a wide range of conjugated frameworks were designed and studied to enhance device performance (*24*, *25*). In addition, approaches have been invented to improve intermolecular packing through controlled thin-film deposition techniques. For instance, Giri and coworkers (*26*) demonstrated that solution shearing could incrementally change the molecular packing of 6,13-bis(triisopropylsilylethynyl)pentacene to achieve a maximum mobility as high as 4.6 $cm^2 V^{-1} s^{-1}$. Furthermore, they invented micropillar-patterned shearing blades, which significantly improved the thin-film morphology, and as a result, the hole mobility for thin films of 6,13-bis(triisopropylsilylethynyl)pentacene reached 11 $cm^2 V^{-1} s^{-1}$ (*27*).

Semiconducting conjugated polymers, in particular donor-acceptor (D-A) polymers, have also been intensively investigated because (i) they can be easily solution-processed to form thin films and (ii) their electronic structures and interchain π-π interactions can be tuned by varying the building blocks of the polymer backbone and molecular engineering of side chains. A number of conjugated polymers exhibiting *p*-type, *n*-type, and even ambipolar semiconducting behavior have been reported (*7*, *24*, *25*, *28*, *29*). Tseng *et al.* (*28*) successfully achieved uniaxial alignment of the polymer poly[4-(4,4-dihexadecyl-4*H*-cyclopenta-[1,2-*b*:5,4-*b*′]dithiophen-2-yl)-alt-[1,2,5]thiadiazolo[3,4-*c*]pyridine] (PCDTPT) into highly oriented fibers by combining nanogrooved substrates and slow-drying in a tunnel-like configuration, and reported high hole mobility up to 23.7 $cm^2 V^{-1} s^{-1}$. High charge carrier mobility was also obtained for conjugated polymers by using capillary action to induce the self-assembly of polymer chains into macroscopically aligned nanostructures (*29*). Note that several of these high-mobility D-A copolymers lack significant long-range order and are nearly amorphous, but they outperform the highly ordered, semicrystalline, polythiophene-based polymers (*30*, *31*). In a recent study, Venkateshvaran *et al.* (*32*) concluded that (i) these polymers display a low degree of energetic disorder and (ii) charge transport in these polymers occurs predominantly along the conjugated polymer backbone and requires only occasional intermolecular hopping via interchain π-π stacking.

Charge-transfer doping with *p*- and *n*-dopants has been intensively investigated as a means of controlling threshold voltages, on/off ratios, and charge mobilities of organic and polymeric semiconductors (*33*–*38*). Such chemical charge-transfer doping would induce the formation of more mobile carriers in the organic semiconductor and increase the conductivity. Enhancement of charge mobility has indeed been observed in some chemically doped organic semiconductors, but the I_{on}/I_{off} ratio is reduced concomitantly after chemical doping (*33*, *35*, *38*).

Incorporation of additives into the electron D-A blending systems has been widely used to optimize phase separation and thus enhance power conversion efficiencies for photovoltaic cells (*39*, *40*). Such a physical blending approach without involving charge-transfer doping has also been explored for organic semiconductors to improve their semiconducting performances, but with limited success. So far, only a few additives have been demonstrated to be able to enhance charge

[1]Beijing National Laboratory for Molecular Sciences, Organic Solids Laboratory, Institute of Chemistry, Chinese Academy of Sciences, Beijing 100190, China. [2]Cavendish Laboratory, University of Cambridge, J. J. Thomson Avenue, Cambridge CB3 0HE, UK.
*These authors contributed equally to this work.
†Corresponding author. Email: dqzhang@iccas.ac.cn (D.Q.Z.); hs220@cam.ac.uk (H.S.); zitong_@iccas.ac.cn (Z.T.L.)

Downloaded from http://advances.sciencemag.org/ on June 26, 2019

carrier mobilities of organic and polymeric semiconductors, and for the most part, the achievable mobilities even after incorporation of these additives are still rather low (*41*–*44*). Smith and coworkers (*42*) have achieved a hole mobility enhancement by blending small conjugated molecules [for example, 2,8-difluoroanthra[2,3-*b*:6,7-*b*′] dithiophene-5,11-diyl)bis(ethyne-2,1-diyl))bis(triethylsilane) (diF-TES-ADT)] with conjugated polymers such as poly(dimethyltriarylamine) and poly (dialkylfluorene-co-dimethyltriarylamine). The enhancement of charge carrier mobility has been reported in a few cases (*45*) by addition of nonsolvents to solutions of conjugated D-A polymers to induce aggregation and improve nanostructural order and interchain π-π interactions. Organic semiconductor/dielectric polymer blends with vertical phase separation have been successfully used to fabricate field-effect transistors (FETs); the charge carrier mobility has been found to be dependent on the molar fraction of the dielectric polymer in the blending thin film, but the resulting peak mobility is still low (*46*). Treat *et al.* (*47*) have successfully used minute amounts of commercially available nucleating agents, which were originally designed for melt solidification of isotactic polypropylene, to efficiently manipulate the solidification kinetics of small molecules and polymeric semiconductors. The application of these nucleating agents creates a new way to fabricate thin-film transistors with uniform electrical characteristics at high yield. However, the presence of such nucleating agents in the semiconducting thin films cannot lead to mobility enhancement.

During our studies on conjugated D-A polymers with positively charged moieties in the side chains, we accidently discovered that incorporation of ammonium salts into certain conjugated D-A polymers can improve the interchain packing order and enhance their charge carrier mobilities. Here, we report the finding that the charge carrier mobility of thin films of the conjugated polymer [poly-[2,5-bis(2-octyldodecyl)-3,6-di(thiophen-2-yl)pyrrolo[3,4-*c*]pyrrole-1,4(2*H*,5*H*)-dionel-alt-thieno[3,2-*b*]thiophene] (DPPTTT; see Fig. 1) can be remarkably enhanced by co-depositing the polymer with an ionic additive, tetramethylammonium iodide (NMe_4I), without extra treatments. Structural and spectroscopic studies were performed to understand the origin of such improvement of charge transport within the polymer thin film after introducing NMe_4I.

RESULTS AND DISCUSSION

Charge carrier mobility of the neat DPPTTT film

The conjugated D-A polymer under investigation is DPPTTT (Fig. 1), which was prepared and purified according to the reported procedures (*48*, *49*). The structural data were identical with those reported previously (*48*, *49*). M_w (weight-average molecular weight) of DPPTTT was measured to be 225 kD with a polydispersity of 2.7. The bottom-gate/bottom-contact (BGBC) FETs with thin films of DPPTTT were fabricated with conventional techniques (see Materials and Methods). As expected, typical *p*-type semiconducting behavior was observed on the basis of the transfer and output curves (see Fig. 2). The hole mobility was estimated to be 1.2 $cm^2 V^{-1} s^{-1}$ based on the plot of $I_{DS}^{1/2}$ versus V_{GS} for the as-prepared device, and it increased to 9.8 $cm^2 V^{-1} s^{-1}$ after thermal annealing at 180°C for 1.0 hour under vacuum. These performance data are almost the same as those reported by Li and coworkers (*49*). We note that the transfer characteristics are not ideal and typically exhibit a region of higher slope at low gate voltage and a region of smaller slope at high gate voltage. Similar non-ideal electrical characteristics have been observed for many DPP-based copolymers, and their origin is currently not clearly understood (*30*, *32*, *48*–*51*). In the absence of an established method of mobility extraction for these materials, we also report below estimated values for mobilities extracted using a very conservative two-point method (see Fig. 3A). This is not meant to be a scientifically rigorous method of mobility extraction, but it provides an important, conservative estimate of the current-carrying performance of the device. The two-point method is essentially providing a conservative estimate of what mobility an ideal transistor with the same geometry and gate dielectric would need to have to generate the same ON current at high gate voltage. In our view, such a conservative cross-check of mobility should always be performed when the measured device characteristics are not ideal.

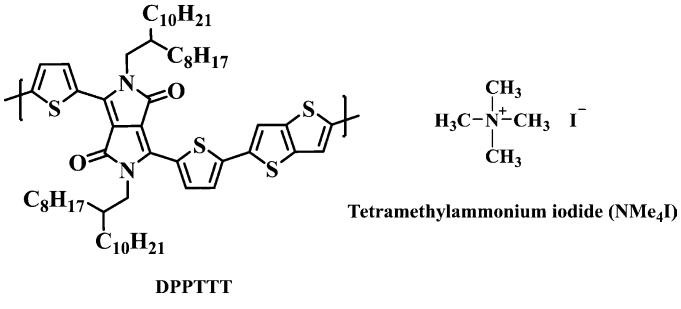

Fig. 1. Chemical structures of DPPTTT and NMe_4I.

Charge carrier mobility of DPPTTT film after incorporation of NMe_4I

Thin films of DPPTTT-NMe_4I were prepared by adding a dimethyl sulfoxide (DMSO) solution of NMe_4I to the hot *o*-dichlorobenzene (*o*-DCB) solution of DPPTTT, followed by spin-coating the hot mixed solution onto the octadecyltrichlorosilane (OTS)–modified SiO_2/Si substrate. The corresponding FETs were fabricated in the same way as with the neat DPPTTT films. The molar ratio between the repeat units of DPPTTT versus NMe_4I was 7.5:1, 15:1, 30:1, and 45:1. On the basis of the output and transfer curves shown for the DPPTTT-NMe_4I thin film of molar ratio 30:1 in Fig. 2, the *p*-type semiconducting property of DPPTTT was retained after addition of NMe_4I. Surprisingly, compared to the pure DPPTTT film, the ON current was enhanced from ~1.1×10^{-4} to ~1.3×10^{-3} A (see Fig. 2). The OFF current also increased about 10-fold, which may be due to broadening the tail of the density of states induced by additive NMe_4I (*52*). This implies that the hole mobility of the DPPTTT-NMe_4I film is significantly higher than that of the neat film. The hole mobility of the DPPTTT-NMe_4I thin film at a molar ratio of 30:1 was first extracted in the manner described above for pure DPPTTT film, namely, the linear part of the plot of $I_{DS}^{1/2}$ versus V_{GS} at low voltages was fitted. Figure 3B shows the distribution of hole mobilities for the DPPTTT-NMe_4I thin film at a molar ratio of 30:1. The average μ_h was estimated to be 19.5 $cm^2 V^{-1} s^{-1}$, which was 24 times higher than that of the pure DPPTTT film without thermal annealing. Notably, the highest μ_h was 26.2 $cm^2 V^{-1} s^{-1}$. It should be pointed out that the transfer curves for the DPPTTT-NMe_4I films were again not ideal, being similar to those for neat DPPTTT film (*49*). Efforts were made to improve the ideality of the transfer curve. For instance, the dielectric layer was changed to a CYTOP/SiO_2 layer. As shown in fig. S1, the deviation of the resulting plot of $I_{DS}^{1/2}$ versus V_{GS} from the linearity became less prominent for both films. We note that (i) such remarkable enhancement of charge mobility by incorporation of NMe_4I was to the

Downloaded from http://advances.sciencemag.org/ on June 26, 2019

best of our knowledge never reported and (ii) high hole mobility up to 26.2 $cm^2 V^{-1} s^{-1}$ was achieved without thermal annealing or any other posttreatments in ambient atmosphere. Alternatively, the hole mobility was also estimated more conservatively. Two points at V_{Th} and V_{GS} = −30 V of the plot of $I_{DS}^{1/2}$ versus V_{GS}, which is out of the linear range (see Fig. 3A), were selected, and μ_h was estimated to be 4.4 $cm^2 V^{-1} s^{-1}$ in this way for the DPPTTT-NMe_4I film. This value provides a lower limit estimate of the mobility and a robust estimate of the current-carrying ability of the device at high gate voltages that can be compared to other OFETs with more ideal characteristics. In the same manner, a hole mobility of 0.8 $cm^2 V^{-1} s^{-1}$ was obtained for the neat DPPTTT thin film without thermal annealing. Figure 3C shows the distribution of hole mobilities for the DPPTTT-NMe_4I thin film at a molar ratio of 30:1, which were estimated with the two-point method. In this way, the average mobilities of the DPPTTT-NMe_4I (at a molar ratio of 30:1) and neat thin films were estimated to be 3.6 and 0.6 $cm^2 V^{-1} s^{-1}$, respectively. Again, the hole mobility of the DPPTTT thin film increased by a factor of 6 after the addition of NMe_4I. Because the choice of gate voltage in the two-point mobility extraction method is arbitrary, we also selected two other points (at V_{Th} and V_{GS} = −20 V and V_{Th} and V_{GS} = −40 V; see fig. S2). The estimated mobilities listed in table S1 depend weakly on the choice of gate voltage, but the enhancement of hole mobility for the DPPTTT thin film after incorporation of NMe_4I is clearly observed for all cases. The hole mobility of DPPTTT-NMe_4I thin film was kept nearly unaltered after thermal annealing at 80°C, but it started to decrease after further thermal annealing at 100° and 120°C (see fig. S3).

Hole mobilities of DPPTTT-NMe_4I thin films at other molar ratios were also extracted by the two methods (see fig. S4) and are listed in Table 1. Hole mobilities were found to be enhanced by incorporating NMe_4I for all molar ratios. The highest performance enhancement was observed at a molar ratio of 30:1. I_{on}/I_{off} ratios for DPPTTT-NMe_4I thin films at molar ratios of 45:1 and 30:1 were found to be in the range of 10^6 to 10^7 as for the neat DPPTTT thin film, whereas those for DPPTTT-NMe_4I thin film at molar ratios of 15:1 and 7.5:1 were lowered to 10^5 to 10^6 and 10^3 to 10^4 (see Table 1), respectively. This was caused by the large enhancement of I_{off} (see Table 1). Such I_{off} enhancement can be interpreted as follows: when more NMe_4I is incorporated into the DPPTTT thin film, the Coulomb wells associated with the iodide anions begin to overlap, leading to a reduction of the barrier height for charge hopping and broadening the tail of the density of states, which is expected to induce an increase in conductivity (*52*).

Apart from NMe_4I, tetramethylammonium bromide (NMe_4Br) was also examined as an additive incorporated into the DPPTTT thin film in the same way. Figure S5 shows the transfer and output curves for the FET with the DPPTTT-NMe_4Br at a molar ratio of 30:1. The hole mobility of the as-prepared FET with DPPTTT-NMe_4Br was obtained by fitting the linear part of the plot of $I_{DS}^{1/2}$ versus V_{GS} (see fig. S5). The highest and average mobilities were determined to be

Downloaded from http://advances.sciencemag.org/ on June 26, 2019

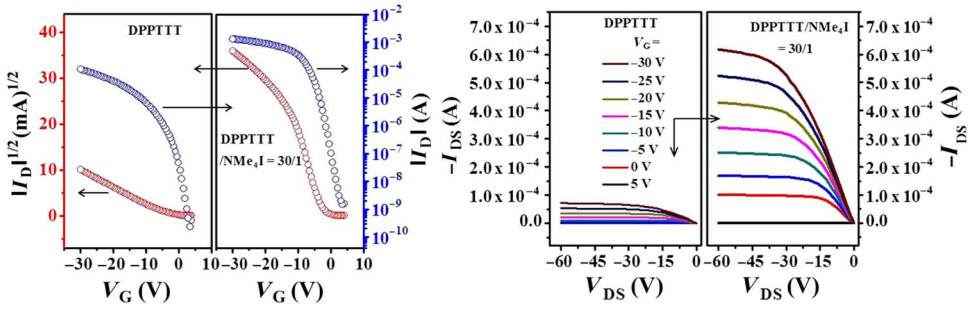

Fig. 2. OFET characteristics for DPPTTT and DPPTTT-NMe_4I. Transfer (V_{DS} = −60 V) and output characteristics of neat DPPTTT and DPPTTT-NMe_4I at a molar ratio of 30:1; the transistor channel width (*W*) and channel length (*L*) were 8800 and 80 μm, respectively.

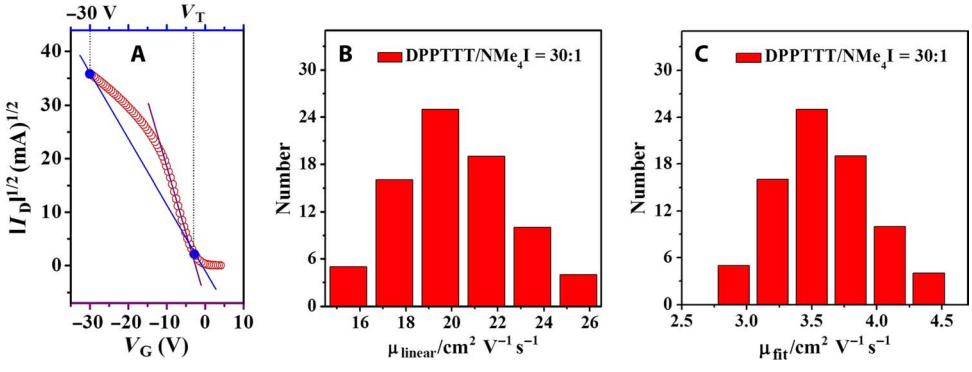

Fig. 3. Transfer characteristics and mobility distribution for DPPTTT-NMe_4I. (**A**) Hole mobilities were extracted in two ways: (i) fitting the linear part of the plot of $I_{DS}^{1/2}$ versus V_{GS} (purple line) and (ii) taking the two points at V_{Th} and V_{GS} = −30 V of the plot of $I_{DS}^{1/2}$ versus V_{GS} (blue line) to provide a very conservative estimate of hole mobility. (**B**) Hole mobility (obtained by fitting the linear part of the plot of $I_{DS}^{1/2}$ versus V_{GS}) distribution for the DPPTTT-NMe_4I thin films at a molar ratio of 30:1. (**C**) Hole mobility (obtained by conservative estimate) distribution for the DPPTTT-NMe_4I thin films at a molar ratio of 30:1.

Table 1. The mobilities (μ), threshold voltages (V_{Th}), on/off ratios (I_{on}/I_{off}), I_{off}, and subthreshold slop (*S*) for as-prepared BGBC FET devices.

	DPPTTT*	DPPTTT/NMe_4I *†			
		7.5	15	30	45
$\mu^{‡}$ ($cm^2\ V^{-1}\ s^{-1}$)	0.8 (2.1)	8.1 (12.9)	15.4 (20.1)	19.5 (26.2)	13.6 (17.3)
$\mu^{§}$ ($cm^2\ V^{-1}\ s^{-1}$)	0.6 (0.8)	1.6 (2.2)	2.8 (3.8)	3.6 (4.4)	2.4 (3.5)
V_{Th} (V)	−4 to 2	−1 to 2	−3 to 1	−3 to 1	−3 to 2
I_{on}/I_{off} (log_{10})	6–7	3–4	5–6	6–7	6–7
I_{off} (A) (average)	5.5×10^{-10}	8.5×10^{-7}	5.4×10^{-8}	6.1×10^{-9}	2.5×10^{-9}
S ($V\ decade^{-1}$)	3–3.2	0.9–1.1	1.0–1.4	1.0–1.2	1.0–1.3

*All data were obtained in air based on more than 50 FET devices with $W = 8800$ μm and $L = 80$ μm at $V_{DS} = -60$ V. †Molar ratio of the repeat moiety of DPPTTT versus NMe4I. ‡Hole mobility, extracted by fitting the linear part of the plot of $I_{DS}^{1/2}$ versus V_{GS}, in the form of average (high). §Hole mobility, on the basis of two points of the plot of $I_{DS}^{1/2}$ versus V_{GS} at V_{Th} and $V_{GS} = -30$ V using the equation $I_{DS} = C_i\mu(V_{GS} - V_{Th})^2W/2L$ (see text), in the form of average (high).

13.7 and 9.2 $cm^2\ V^{-1}\ s^{-1}$, respectively, being ca. 6 and 11 times those the neat DPPTTT thin film.

The possible effect of DMSO, which was used to dissolve NMe_4I, on the enhancement of charge carrier mobility was examined by performing control experiments without NMe_4I. The same volumes of DMSO were added to the same *o*-DCB solution of DPPTTT as for the preparation of the respective DPPTTT-NMe_4I thin films at different molar ratios, followed by spin-coating the solutions on the same substrates and fabrication of FETs in the same manner as for DPPTTT-NMe_4I thin films. As depicted in fig. S6, the respective transfer curves were well overlapped with that of the neat DPPTTT thin film without using DMSO as a co-solvent. Clearly, the thin-film hole mobility was not affected by the addition of DMSO.

The operational stability of DPPTTT-NMe_4I FETs was also found to be good. As an example, the ON current I_{on} and OFF current I_{off} of DPPTTT-NMe_4I at a molar ratio of 30:1 remained relatively constant when switching the device ON (−30 V) and OFF 300 times as depicted in Fig. 4A. Figure 4B shows the variation of hole mobility and I_{on}/I_{off} after the devices were left in air for different periods. μ_h decreased slightly after the device had been left in air for 6 days and then remained almost unaltered even after 60 days. Therefore, the device air stability of the DPPTTT-NMe_4I thin films was satisfactory.

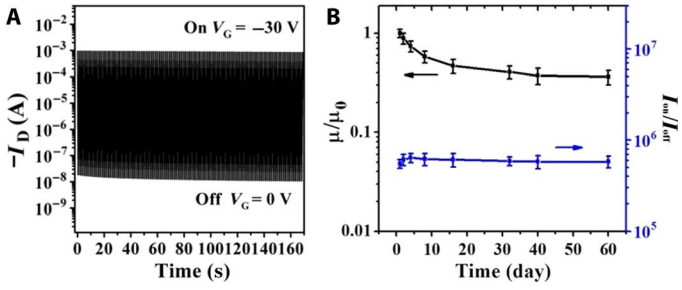

Fig. 4. Operational stability of OFETs with DPPTTT-NMe_4I thin films. (**A**) Cyclic stability of a representative device with the DPPTTT-NMe_4I thin film at a molar ratio of 30:1 showing maintenance of ON and OFF currents during 300 continuous on/off cycles. (**B**) Variation of hole mobility and I_{on}/I_{off} for DPPTTT-NMe_4I FET at a molar ratio of 30:1 after the device was left in air for different periods.

Mechanism for the remarkable mobility enhancement

Possible mechanisms for such mobility enhancement by incorporation of NMe_4I may include (i) a contribution of ionic conductivity, (ii) a chemical charge-transfer doping of the organic semiconductor, (iii) a beneficial effect of the ionic additive on the thin-film morphology and/or microstructure of the polymer, or (iv) a doping-induced reduction of contact resistance.

If the drift of ions and ionic conductivity would make a significant contribution to the mobility enhancement under FET operational conditions, significant hysteresis would be expected between the output/transfer curves measured with forward and reverse voltage sweeps. Figure S7 shows the initial transfer/output curves for DPPTTT-NMe_4I (30:1) thin film and those after the third, fifth, seventh, and tenth forward voltage sweep. It is clear that these output/transfer curves almost overlap. For comparison, the corresponding transfer/output curves were also measured for neat DPPTTT thin films in the same way; as shown in fig. S7, the initial output/transfer curves are almost the same as those after continuous forward voltage sweeps. Furthermore, hysteresis is rather small for both the transfer and output curves measured with forward and reverse voltage sweeps for DPPTTT-NMe_4I thin film as shown in fig. S8. On the basis of these results, it can be concluded that the possible contribution of the drift of ions and ionic conductivity to the enhancement of charge carrier mobility can be neglected.

Spectroscopic studies

Ultraviolet-visible (UV-vis) absorption, infrared (IR), Raman, and electron spin resonance (ESR) spectra were measured for neat and DPPTTT-NMe_4I films. As depicted in fig. S9, no ESR signals from NMe_4I-induced polarons were detected in any of the films. Moreover, UV-vis absorption, IR, and Raman spectra of DPPTTT-NMe_4I films overlapped well with those of the pure films, as shown in fig. S10. These results manifest that the electronic structure of DPPTTT was not affected by the presence of NMe_4I, and chemical charge-transfer doping did not occur. This conclusion was further corroborated by photothermal deflection spectroscopy (PDS) measurements, which were performed with the neat DPPTTT thin film and the DPPTTT-NMe_4I thin film at a molar ratio of 30:1. Figure 5 shows the PDS spectra of both thin films. The samples showed no discernable changes, in particular, no evidence for polaron-induced absorptions in the

Downloaded from http://advances.sciencemag.org/ on June 26, 2019

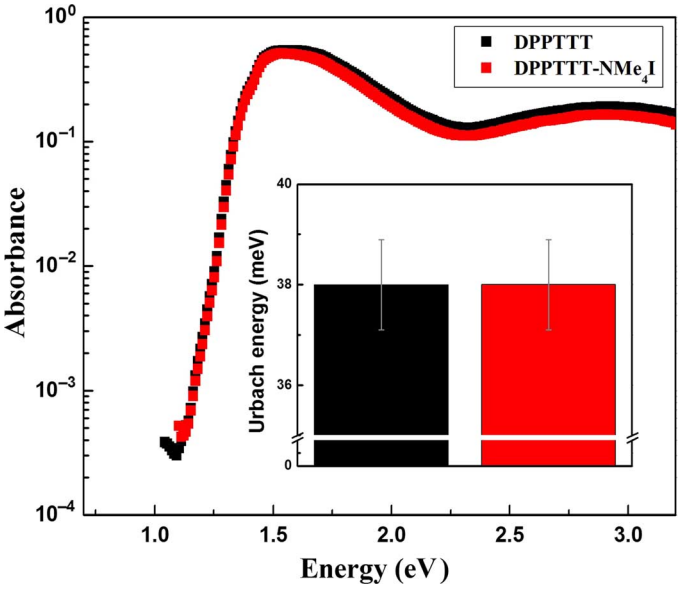

Fig. 5. PDS spectra of DPPTTT and DPPTTT-NMe_4I thin films. PDS spectra of thin films of DPPTTT and DPPTTT-NMe_4I at a molar ratio of 30:1. The inset shows the respective Urbach energies.

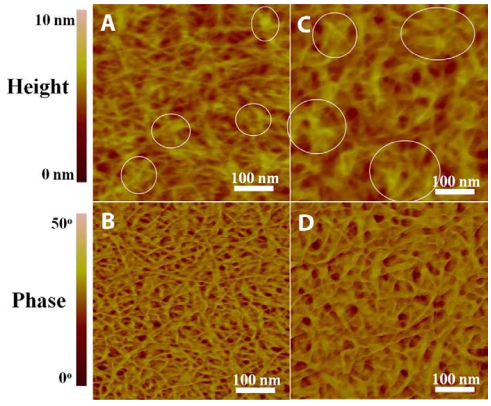

Fig. 6. AFM images of DPPTTT and DPPTTT-NMe_4I. (**A** to **D**) AFM height and phase images of the neat DPPTTT thin film (A and B) and the DPPTTT-NMe_4I thin film at a molar ratio of 30:1 (C and D). The circles in (C) highlight the formation of more connected and larger fiber aggregates within the DPPTTT-NMe_4I thin film in comparison with those marked by circles in (A) for the neat DPPTTT thin film.

sub-bandgap absorption region. This also indicates that the NMe_4I additive does not act as a chemical dopant of DPPTTT and does not alter the electronic structure of the polymer materially. This is also indicated by the energetic disorder parameter, the Urbach energy, extracted from a linear fit to the exponentially decaying sub-bandgap tail of the PDS absorption edge. The Urbach energy provides an empirical way of assessing energetic disorder in the polymer semiconductor due to variations in backbone conformation that have been found to correlate with the field-effect mobilities observed in polymer FETs (*32*, *53*). The estimated Urbach energy for both the neat film and the films with NMe_4I was 38 meV (see inset of Fig. 5), which is a relatively low value compared to most conjugated D-A polymers, although not as low as in the polymers with the lowest degree of energetic disorder (*32*). Such low Urbach energy indicates that DPPTTT exhibits a relatively low degree of energetic disorder and that the NMe_4I additive does not change the degree of energetic disorder in DPPTTT.

Thin-film morphology

Morphological changes of the polymer films after addition of NMe_4I were explored with atomic force microscopy (AFM). Both the height and phase images (Fig. 6) show that the neat thin film of DPPTTT contains interconnected fibers with an average width of ca. 8 nm and some fibers are aggregated. After incorporation of NMe_4I, the fibers of similar size are kept, but large fiber aggregates are formed (see highlighted circles in Fig. 6). We currently cannot conclude that the appearance of large fiber aggregates within DPPTTT-NMe_4I thin film is beneficial for charge transport because it is reported that much of the charge transport occurs along individual polymer chains and only requires intermittent connectivity to other chains according to recent studies (*31*, *54*, *55*).

Interchain packing order

Grazing incidence wide-angle x-ray scattering (GIWAXS) measurements were performed for the neat DPPTTT and DPPTTT-NMe_4I films. Figure 7 shows the two-dimensional (2D) GIWAXS patterns and the respective profiles along the Q_z and Q_{xy} directions. As depicted in Fig. 7, the neat thin film showed one scattering peak along the Q_z direction at Q_z = ca. 0.33 $Å^{-1}$ and a weak one at Q_z = ca. 0.63 $Å^{-1}$, corresponding to the intermolecular polymer chain packing distance of ca. 19.3 Å, which was rather close to that reported previously (*49*). However, for the DPPTTT-NMe_4I thin film, four orders of scattering signals along the Q_z direction were observed; apart from the first peak at Q_z = ca. 0.33 $Å^{-1}$ with a *d*-spacing of ca. 19.3 Å, the second-, third-, and fourth-order scattering peaks at Q_z = ca. 0.63 $Å^{-1}$, Q_z = ca. 0.92 $Å^{-1}$, and Q_z = ca. 1.25 $Å^{-1}$, respectively, emerged after incorporation of NMe_4I (see Fig. 7C). Obviously, the degree of order for the lamellar edge-on stacking of the alkyl chains increases for the DPPTTT-NMe_4I thin film. Moreover, the DPPTTT-NMe_4I thin film exhibited a scattering signal at Q_{xy} = ca. 1.60 $Å^{-1}$, corresponding to a *d*-spacing of ca. 3.9 Å in the in-plane direction (see Fig. 7D). In addition, a weak peak Q_z = ca. 1.60 $Å^{-1}$ in the out-of-plane was detected after incorporation of NMe_4I (see Fig. 7C). These GIWAXS data indicate the appearance of interchain stacking for the DPPTTT-NMe_4I thin film. In comparison, the neat DPPTTT thin film showed no scattering signals higher than 1.50 $Å^{-1}$ in both the out-of-plane and in-plane directions. These results reveal that the incorporation of NMe_4I can improve the packing order degree for both side alkyl chains and the interchain stacking of the conjugated backbones.

Theoretical calculation

To better understand the improvement of the degree of order in the lamellar stacking of the alkyl side chains and interchain stacking in the presence of NMe_4I, we performed theoretical calculations for two repeat units of DPPTTT; three branching alkyl chains were replaced separately by three $-CH_2CH_3$, and each of the two long alkyl chains of the fourth branching group was replaced by $-CH_2CH_2CH_3$ to simplify the calculations. The molecular geometries of DPPTTT alone and after incorporation of either I^- or NMe_4^+ were optimized by density functional theory using the B3LYP functional with the MidiX basis set for I^- and 6-31G* basis set for other atoms. The

Downloaded from http://advances.sciencemag.org/ on June 26, 2019

polarizable continuum model with *o*-DCB as solvent was implemented to take account of the environmental dielectric effects. As depicted in Fig. 8A, the most negative electrostatic potential (ESP) is around the carbonyl groups of DPP moieties, whereas the most positive ESP is around the thienothiophene moieties. According to the ESP map, iodide and tetramethylammonium ions were put close to the thienothiophene and carbonyl groups, respectively. Then, the conformation was further optimized, and the resulting energetically stable conformation is shown in Fig. 8B. This is indeed consistent with the observation that the ^{13}C nuclear magnetic resonance (NMR) relaxation times of carbon atoms of the side alkyl chains are shortened for the DPPTTT-NMe_4I film in comparison with those for the neat film (table S2).

The dihedral angle between the side chain and the polymer backbone was altered consecutively. During rotation, the polymer backbone and I^- or NMe_4^+ were fixed, whereas the side chain was relaxed. The calculated torsion potentials are shown in Fig. 8C. Apparently, in the presence of I^- or NMe_4^+, the variation of torsion potential versus the dihedral angle (between the side chain and the conjugated backbone) is much steeper with

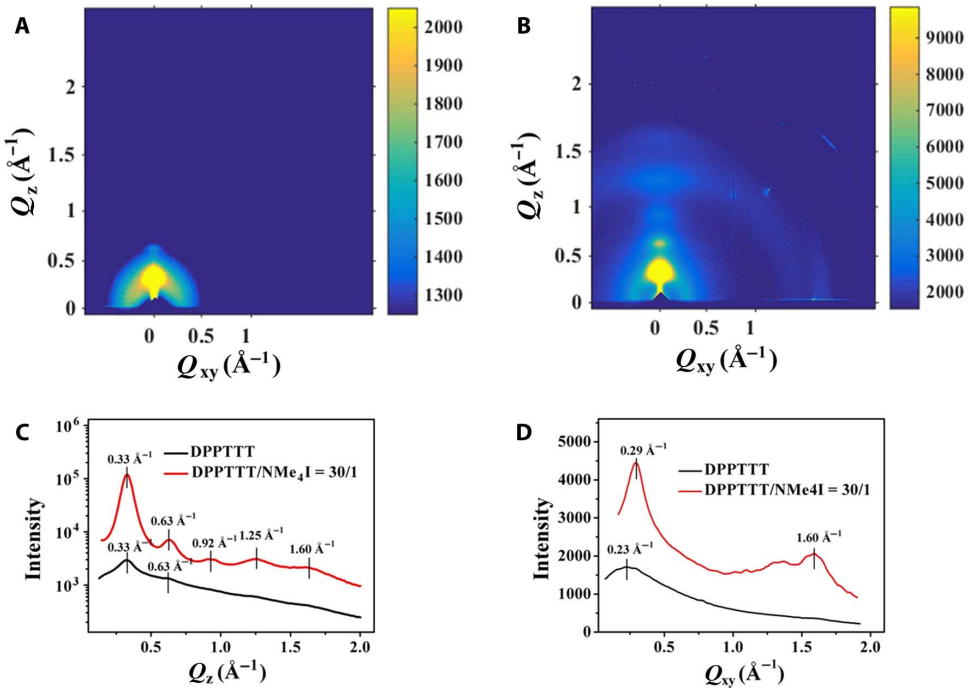

Fig. 7. GIWAXS patterns of DPPTTT and DPPTTT-NMe_4I thin films. (**A** and **B**) 2D GIWAXS images of DPPTTT (A) and DPPTTT-NMe_4I (B) at a molar ratio of 30:1. (**C**) Out-of-plane linecuts of 2D GIWAXS of DPPTTT and DPPTTT-NMe_4I at a molar ratio of 30:1. (**D**) In-plane linecuts of 2D GIWAXS of DPPTTT-NMe_4I at a molar ratio of 30:1.

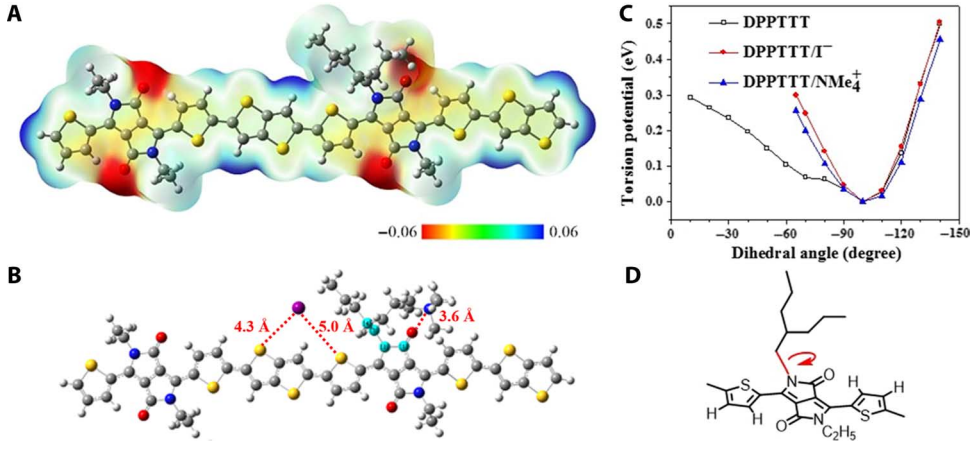

Fig. 8. Theoretical calculation of the torsion of the side alkyl chains. (**A**) The ESP map of DPPTTT (in unit of Hartree); the unit is elementary charge. (**B**) Illustration of the positions (including the interatomic distances) of I^- and NMe_4^+ on DPPTTT and the rotation angle of the side alkyl chain that is highlighted in cyan. (**C**) The variation of the calculated torsion potential versus the dihedral angle between the side chain and conjugated backbone for neat DPPTTT and those after incorporation of either I^- or NMe_4^+. (**D**) Schematic diagram of the torsion of the alkyl chain and indication of the dihedral angle.

Downloaded from http://advances.sciencemag.org/ on June 26, 2019

respect to the neat DPPTTT; thus, the rotation of the side chain can be restricted to some extent, and the number of accessible conformations for the side chain of DPPTTT should be reduced.

Scanning Kelvin probe microscopy characterization

To examine the effect of the incorporation of NMe_4I on the interfacial contact resistance between the drain/source electrodes and semiconducting film, the potential profiles across the channel were measured using scanning Kelvin probe microscopy (SKPM) under different gate voltages for both the neat and DPPTTT-NMe_4I thin films. The source electrode was grounded, and the drain was kept constant at −4 V when the gate was varied. It is obvious that potential drops were detected at the interfaces between source/drain electrodes and semiconducting films when the gate voltage was low for the neat thin film (see fig. S11). This is due to the existence of contact resistance. As the gate voltage increased, the potential drop became less obvious, implying the reduction of contact resistance due to conductivity enhancement. However, for the DPPTTT-NMe_4I thin film, no potential drops were observed at the respective interfaces between source/drain electrodes and semiconducting films at different gate voltages as shown in fig. S11. The potential decreased from source electrode to drain electrode uniformly, and the potential profiles were almost independent of the gate voltage. The results manifest that the contact resistance was largely reduced in the DPPTTT-NMe_4I film. This may be caused by the enhancement of thin-film conductivity reflected by the slight enhancement of the OFF current in the transfer curves (see Fig. 2). This reduction of contact resistance is expected to enhance the charge mobility. However, a quantitative analysis of the contact resistance–corrected potential drops along the channel shows that the charge mobility is expected to be enhanced only by factors of 1.3 to 1.9 as a result of the lower contact resistance in the DPPTTT-NMe_4I films (see fig. S12).

On the basis of these characterization results, the enhancement of charge carrier mobility for DPPTTT film upon addition of NMe_4I can be rationalized as follows. The reduction of contact resistance can only partly account for the improved charge mobility in the DPPTTT-NMe_4I films. The improvement of the degree of edge-on lamellar packing of the alkyl side chains and interchain π-π stacking is likely to be the most important factor responsible for the improvement in charge mobility. The theoretical simulations show that the I^- and NMe_4^+ ions are expected to inhibit the torsion of the alkyl side chains and in this way improve the lamellar side chain packing and interchain π-π stacking. To conclude, the incorporation of NMe_4I into thin film of DPPTTT can lead to (i) improvement of conductivity and reduction of contact resistance and (ii) inhibition of the torsion of side alkyl chains and facilitation of the orderly lamellar arrangement of the alkyl side chains and interchain π-π stacking. The formation of large fiber aggregates after incorporation of NMe_4I may also facilitate charge transport. These facts work synergistically and lead to the remarkable enhancement of charge carrier mobility.

Charge carrier mobility enhancement for other conjugated D-A polymers after incorporating NMe_4I

On the basis of the above understanding, we investigated whether this strategy with NMe_4I can be applied to other conjugated polymers to improve charge carrier mobilities. BGBC FETs with thin films of PDPP4T, PBDTTT-C-T, P3HT, and P3EHT (Fig. 9) and the respective thin films after incorporation of NMe_4I at a molar ratio of 30:1 (the respective repeat unit versus NMe_4I) were fabricated. On the basis of the respective transfer curves (see fig. S13), which were measured without thermal annealing, hole mobilities of the respective neat films and those after incorporation of NMe_4I were extracted as listed in table S3. Note that hole mobility of PDPP4T (obtained by fitting the linear part of the plot of $I_{DS}^{1/2}$ versus V_{GS} at low voltages) increased from 0.8 $cm^2\ V^{-1}\ s^{-1}$ for the neat film to 8.1 $cm^2\ V^{-1}\ s^{-1}$ after addition of NMe_4I. Hole mobilities were also estimated conservatively as described above; in this manner, hole mobility of PDPP4T thin film was again enhanced by about four times after incorporation of NMe_4I (see table S3). The hole mobility enhancement (about fourfold) was also observed for PBDTTT-C-T after addition of NMe_4I. However, hole mobility of both P3HT and P3EHT decreased upon incorporation of NMe_4I (see table S3). Like DPPTTT, PDPP4T and PBDTTT-C-T are conjugated D-A polymers with branched side alkyl chains, whereas P3HT and P3EHT contain just thiophene moieties with linear alkyl chains and branched alkyl chains, respectively. This shows that our simple approach of incorporating an ionic additive, NMe_4I, for enhancing hole mobility is applicable to a range of conjugated D-A polymers with branched side alkyl chains, but does not provide a universal benefit for all conjugated polymers.

CONCLUSION

To conclude, we report the discovery that the charge mobility of the conjugated D-A polymer DPPTTT can be remarkably enhanced by addition of ionic NMe_4I. The hole mobility of the DPPTTT-NMe_4I at a molar ratio of 30:1 is increased by more than an order of magnitude over that of the neat films without extra thermal treatments and reaches very high values of 4.4 $cm^2\ V^{-1}\ s^{-1}$ (when estimated conservatively) or 26.2 $cm^2\ V^{-1}\ s^{-1}$, respectively (when estimated from a narrow gate voltage range near the turn on). Spectroscopic studies conclude that this improvement is not due to chemical charge-transfer doping. Instead, on the basis of GIWAXS and theoretical studies, we reason that this mobility enhancement is induced by the inhibition of the torsion of the branching alkyl chains due to the presence of iodide and tetramethylammonium ions and consequent facilitation of the formation of an ordered lamellar packing of the alkyl side chains benefiting the interchain π-π interactions. Our results identify the use of ionic additive as a powerful method for improving the microstructural order and charge transport properties of the conjugated D-A polymer DPPTTT. This simple approach is also applicable to other conjugated D-A polymers for improving charge carrier mobilities.

MATERIALS AND METHODS

Materials and characterization techniques

NMe_4I was purchased from Aldrich without further purification. PDPP4T, PBDTTT-C-T, P3HT, and P3EHT were purchased from Solarmer Materials Inc. DPPTTT was prepared and purified according to the reported procedures (*48*, *49*). M_w was determined by gel permeation chromatography at 140°C on a PL-220 system using three PLgel Olexis columns and 1,2,4-trichlorobenzene as eluent; a flow rate of 1 ml min^{-1} was used.

^1H and ^{13}C NMR spectra were recorded on Bruker Avance 500 and Bruker Avance 400 spectrometers. Absorption spectra were

Downloaded from http://advances.sciencemag.org/ on June 26, 2019

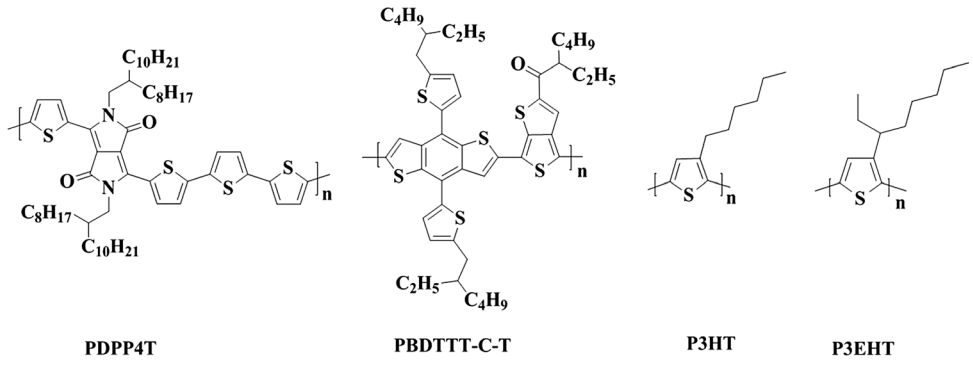

Fig. 9. Chemical structures of PDPP4T, PBDTTT-C-T, P3HT, and P3EHT.

measured using a Jasco V-570 UV-Vis spectrophotometer. IR and Raman spectra were measured using TENSOR 27 (Bruker) and RFS 100/S (Bruker), respectively. ESR spectra were recorded on ESP 300 (Bruker). AFM images were recorded on a Nanoscope III AFM in trapping mode. GIWAXS measurements were conducted at the 8-ID-E beamline (*56*) at the Advanced Photon Source, Argonne National Laboratory, using x-rays with a wavelength of λ = 1.6868 Å and a beam size of ~200 μm (*h*) and 20 μm (*v*). PDS was performed as reported before (*53*). Thin film thicknesses were measured using a profilometer (Ambios Technology XP-2). The x-ray photoelectron spectroscopy (XPS) measurements were performed on the ESCALAB 250Xi XPS system. Capacitance at different frequencies (1 to 2000 Hz) was measured on NF ZM2371 LCR meter.

Fabrication of OFET devices

A heavily *n*-doped Si wafer with a 300-nm SiO_2 surface layer (respective capacitance of 11 nF·cm^{-2}) was used as the substrate, with Si wafer serving as a common gate electrode and SiO_2 as the dielectric. For the OTS self-assembled monolayer modification, the Si wafer surface was first cleaned by sonication in acetone and deionized water for 5.0 min sequentially and then immersed in piranha solution (2:1 mixture of sulfuric acid and 30% hydrogen peroxide) for 20 min under 100°C. This was followed by rinsing with deionized water several times. Then, the silicon wafer was sonicated in deionized water and isopropanol for 5.0 min. After drying by nitrogen blow, the silicon wafer was treated in a vacuum oven at 80°C for 30 min and then modified with OTS (octadecyltrichlorosilane) in a vacuum oven at 125°C for 240 min. OTS-modified silicon wafer was cleaned by sonication in trichloromethane, hexane, and isopropanol separately for 5.0 min in each case and dried by nitrogen blow. The Au source/drain electrodes were then deposited via thermal vacuum evaporation on the substrate through a shadow mask bearing source/drain electrode features of various dimensions. For BGBC devices, DPPTTT was spin-coated from its hot *o*-DCB solution (5.0 mg/ml, 100°C) onto the Au-patterned dielectric surface. During this spin-coating process, the wafer was heated using a hair dryer for 20 s. NMe_4I in DMSO was added to the hot *o*-DCB solution of DPPTTT. This solution was stirred for 5.0 min at 100°C in ambient atmosphere and then spin-coated as before. For the CYTOP/SiO_2 dielectric layer, CYTOP was spin-coated onto the surface of SiO_2, and the CYTOP surface was treated with plasma, followed by modification with OTS; then, the respective solutions were spin-coated onto the surfaces. Thin-film thicknesses, measured using a profilometer (Ambios Technology XP-2), were in the range of 50 to 60 nm for DPPTTT-NMe_4I (45:1), DPPTTT-NMe_4I (30:1), DPPTTT-NMe_4I (15:1), and the neat DPPTTT thin films, whereas that for DPPTTT-NMe_4I (7.5:1) was in the range of 80 to 90 nm. Thin films of DPPTTT and DPPTTT-NMe_4I on the silicon wafers, which were prepared similarly to those for fabrication of FETs, were subjected to XPS analyses. As an example, fig. S14 shows the XPS spectra of core level bands of N 1*s* and I 3*d* (I $3d_{5/2}$ and I $3d_{3/2}$) for DPPTTT-NMe_4I (15:1). The N 1*s* band centered at 402.0 eV was detected for the thin film. This N 1*s* band is due to the nitrogen in NMe_4^+. Simultaneously, the I $3d_{5/2}$ and I $3d_{3/2}$ bands centered at 619.0 and 630.3 eV due to I^- were also detected. Thus, it can be concluded that NMe_4I was retained in the thin film.

To address the possibility of gate-induced drift of ions from the bulk into the interface, which may change the effective capacitance of the device, NMe_4I solutions with different concentrations [0.24, 0.46, and 0.84 μmol/ml in DMSO/*o*-DCB (v/v; 1:20, 1:10, and 1:5, respectively)] were spin-coated onto the OTS-modified SiO_2 dielectric layer in the same way as for the preparations of the DPPTTT-NMe_4I thin films; the concentrations of NMe_4I were the same as those for the preparations of the DPPTTT-NMe_4I thin films with molar ratios of 30:1, 15:1, and 7.5:1. These dielectric layers with NMe_4I were subjected to capacitance measurements at different frequencies (1 to 2000 Hz) with the configuration Au/NMe_4I/OTS-modified SiO_2/Si. The data shown in fig. S15 indicate that (i) the capacitances are frequency-independent and (ii) the capacitances (11.3 ± 0.5 nF·cm^{-2}) are almost the same as those for OTS-modified SiO_2 dielectric layer without NMe_4I. These results reveal that the presence of a small amount of NMe_4I on the dielectric layer does not affect the capacitance. Moreover, DPPTTT solutions were spin-coated onto the OTS-modified SiO_2 with NMe_4I, and the resulting thin films were used to fabricate FETs. As shown in fig. S16, hysteresis in transfer characteristics was clearly observed between the forward and reverse voltage sweeps. Similarly, transfer curves for the neat DPPTTT and DPPTTT-NMe_4I (30:1) thin films (on the OTS-modified SiO_2) were measured with both forward and reverse voltage sweeps. As depicted in fig. S8, the transfer curves between the forward and reverse voltage sweeps were almost overlapped for both neat DPPTTT and DPPTTT-NMe4I (30:1) thin films. These results manifest that NMe_4^+ and I^- ions are mainly retained in the bulk thin films for DPPTTT-NMe_4I and the gate-induced drift of ions from the bulk into the interface can be neglected. Conversely, these data support the conclusion that the presence of NMe_4I in the thin films does not affect the capacitance.

Downloaded from http://advances.sciencemag.org/ on June 26, 2019

Device characterization

Characterization of thin-film FETs was carried out using a Keithley 4200 Semiconductor Characterization System in ambient air. The field-effect mobility in the saturation regime was extracted using the equation $I_{DS} = C_i\mu(V_{GS} - V_{Th})^2W/2L$, under the condition of $-V_{DS} > -(V_{GS} - V_{Th})$. Alternatively, two points corresponding to threshold voltage and $V_{GS} = -30$ V of the plot of $I_{DS}^{1/2}$ versus V_{GS} were selected to estimate the mobility conservatively using the same equation $I_{DS} = C_i\mu(V_{GS} - V_{Th})^2W/2L$, where I_{DS} is the source/drain current, μ is the field-effect mobility, W is the channel width, L is the channel length, C_i is the capacitance per unit area of gate dielectric layer, and V_{GS} (−30 V), V_{Th}, and V_{DS} are the gate, threshold, and source/drain voltages, respectively.

Scanning Kelvin probe microscopy measurement

The SKPM measurement was done using a Veeco Dimension 3100 scanning probe microscopy system in ambient conditions. The SCM-PIT (Pt-Ir; frequency, ~75 kHz; Bruker) tip was used for the SKPM measurement. The drain and gate voltages were provided to the device through a home-made sample holder. In the linear regime, the mobility can be obtained from $\mu = I_{DS}L/[V_{DS}WC_i(V_{GS} - V_{Th})]$. When the contact resistance is taken into account, the value of L/V_{DS} needs to be corrected according to the measured potential profiles, whereas other parameters remain unchanged. With this method, the corrected mobility is dependent on the gate voltage and can be 1.3 to 1.9 times higher than the uncorrected ones at V_{GS} from 0 to −30 V.

SUPPLEMENTARY MATERIALS

Supplementary material for this article is available at http://advances.sciencemag.org/cgi/content/full/2/5/e1600076/DC1

fig. S1. Transfer and output characteristics of FETs with DPPTTT and the DPPTTT-NMe_4I thin film at a molar ratio of 30:1 by using CYTOP-modified dielectric layers.

fig. S2. Extraction of hole mobilities from the transfer characteristics of DPPTTT and DPPTTT-NMe_4I thin film at a molar ratio of 30:1.

fig. S3. Variation of hole mobility for FETs with DPPTTT-NMe_4I thin film at a molar ratio of 30:1 before and after thermal annealing at 80°, 100°, and 120°C.

fig. S4. Transfer characteristics of FETs with DPPTTT-NMe_4I thin films at different molar ratios.

fig. S5. Transfer and output characteristics of FETs with DPPTTT-NMe_4Br thin films at a molar ratio of 30:1.

fig. S6. Transfer characteristics of FETs with DPPTTT thin films without NMe_4I after addition of DMSO to the polymer solutions.

fig. S7. The initial output/transfer curves for DPPTTT and DPPTTT-NMe_4I (30:1) thin film and those after the third, fifth, seventh, and tenth forward voltage sweeps (1st, black; 3rd, blue; 5th, red; 7th, yellow; 10th, cyan).

fig. S8. The transfer and output curves of FETs with DPPTTT-NMe_4I thin films at a molar ratio of 30:1 measured with forward (black) and reverse (blue) voltage sweeps (V_{GS} from 5 to −40 and to 5 V; V_{DS} from 0 to −60 and to 0 V).

fig. S9. ESR spectra of DPPTTT and DPPTTT-NMe_4I.

fig. S10. Absorption, IR, and Raman spectra of thin films of DPPTTT and DPPTTT-NMe_4I at molar ratios of 15:1 and 30:1.

fig. S11. The SKPM potential profiles of DPPTTT and DPPTTT-NMe_4I thin films at a molar ratio of 30:1 under different gate voltages.

fig. S12. The dependence of the ratio of corrected mobility to uncorrected mobility of DPPTTT thin film on the gate voltage.

fig. S13. Transfer characteristics of FETs with other conjugated D-A polymers after incorporation of NMe_4I.

fig. S14. X-ray photoelectron spectra of thin films of DPPTTT and DPPTTT-NMe_4I at a molar ratio of 15:1.

fig. S15. The plot of the capacitances at different frequencies (1 to 2000 Hz) for the dielectric layers measured with the configuration Au/NMe_4I/OTS-modified SiO_2/Si.

fig. S16. Hysteresis in transfer characteristics of FETs with DPPTTT using the NMe_4I-OTS-SiO_2 as the dielectric layer.

table S1. The hole mobilities (μ) extracted by the two-point method with V_{Th} and different values of V_{GS} for as-prepared BGBC FETs with DPPTTT neat film and DPPTTT-NMe_4I at a molar ratio of 30:1.

table S2. Relaxation times of carbon atoms of the side alkyl chains of DPPTTT in the absence and presence of NMe_4I on the basis of solid state of ^{13}C NMR.

table S3. The mobilities (μ), threshold voltages (V_{Th}), on/off ratios (I_{on}/I_{off}), I_{off}, and subthreshold slop (S) for as-prepared BGBC FETs with neat thin films of PDPP4T, PBDTTT-C-T, P3HT, and P3EHT and the respective thin films after incorporation of NMe_4I at a molar ratio of 30:1.

REFERENCES AND NOTES

1. G. Horowitz, Organic field-effect transistors. *Adv. Mater.* **10**, 365–377 (1998).
2. J. Zaumseil, H. Sirringhaus, Electron and ambipolar transport in organic field-effect transistors. *Chem. Rev.* **107**, 1296–1323 (2007).
3. W. Wang, L. Chi, Area-selective growth of functional molecular architectures. *Acc. Chem. Res.* **45**, 1646–1656 (2012).
4. X. Guo, A. Facchetti, T. J. Marks, Imide- and amide-functionalized polymer semiconductors. *Chem. Rev.* **114**, 8943–9021 (2014).
5. A. L. Briseno, S. C. B. Mannsfeld, M. M. Ling, S. Liu, R. J. Tseng, C. Reese, M. E. Roberts, Y. Yang, F. Wudl, Z. Bao, Patterning organic single-crystal transistor arrays. *Nature* **444**, 913–917 (2006).
6. A. B. Mallik, J. Locklin, S. Mannsfeld, C. Reese, M. Roberts, M. Senatore, H. Zi, and Z. Bao, Design, synthesis, and transistor performance of organic semiconductors, in *Organic Thin Film Transistors*, Z. Bao, J. Locklin, Eds. (CRC Press, Boca Raton, FL, 2007).
7. C. Wang, H. Dong, W. Hu, Y. Liu, D. Zhu, Semiconducting π-conjugated systems in field-effect transistors: A material odyssey of organic electronics. *Chem. Rev.* **112**, 2208–2267 (2012).
8. B.-G. Kim, E. J. Jeong, J. W. Chung, S. Seo, B. Koo, J. Kim, A molecular design principle of lyotropic liquid-crystalline conjugated polymers with directed alignment capability for plastic electronics. *Nat. Mater.* **12**, 659–664 (2013).
9. K. Takimiya, S. Shinamura, I. Osaka, E. Miyazaki, Thienoacene-based organic semiconductors. *Adv. Mater.* **23**, 4347–4370 (2011).
10. H. Chen, S. Dong, M. Bai, N. Cheng, H. Wang, M. Li, H. Du, S. Hu, Y. Yang, T. Yang, F. Zhang, L. Gu, S. Meng, S. Hou, X. Guo, Solution-processable, low-voltage, and high-performance monolayer field-effect transistors with aqueous stability and high sensitivity. *Adv. Mater.* **27**, 2113–2120 (2015).
11. Y. Liang, L. Yu, A new class of semiconducting polymers for bulk heterojunction solar cells with exceptionally high performance. *Acc. Chem. Res.* **43**, 1227–1236 (2010).
12. Y. Zhou, C. Fuentes-Hernandez, J. Shim, J. Meyer, A. J. Giordano, H. Li, P. Winget, T. Papadopoulos, H. Cheun, J. Kim, M. Fenoll, A. Dindar, W. Haske, E. Najafabadi, T. M. Khan, H. Sojoudi, S. Barlow, S. Graham, J.-L. Brédas, S. R. Marder, A. Kahn, B. Kippelen, A universal method to produce low–work function electrodes for organic electronics. *Science* **336**, 327–332 (2012).
13. A. T. Yiu, P. M. Beaujuge, O. P. Lee, C. H. Woo, M. F. Toney, J. M. J. Fréchet, Side-chain tunability of furan-containing low-band-gap polymers provides control of structural order in efficient solar cells. *J. Am. Chem. Soc.* **134**, 2180–2185 (2012).
14. J. Peet, A. J. Heeger, G. C. Bazan, "Plastic" solar cells: Self-assembly of bulk heterojunction nanomaterials by spontaneous phase separation. *Acc. Chem. Res.* **42**, 1700–1708 (2009).
15. G. Li, R. Zhu, Y. Yang, Polymer solar cells. *Nat. Photonics* **6**, 153–161 (2012).
16. M. Graetzel, R. A. J. Janssen, D. B. Mitzi, E. H. Sargent, Materials interface engineering for solution-processed photovoltaics. *Nature* **488**, 304–312 (2012).
17. S. Gélinas, A. Rao, A. Kumar, S. L. Smith, A. W. Chin, J. Clark, T. S. van der Poll, G. C. Bazan, R. H. Friend, Ultrafast long-range charge separation in organic semiconductor photovoltaic diodes. *Science* **343**, 512–516 (2014).
18. R. H. Friend, R. W. Gymer, A. B. Holmes, J. H. Burroughes, R. N. Marks, C. Taliani, D. D. C. Bradley, D. A. Dos Santos, J. L. Brédas, M. Lögdlund, W. R. Salaneck, Electroluminescence in conjugated polymers. *Nature* **397**, 121–128 (1999).
19. H. Wu, L. Ying, W. Yang, Y. Cao, Progress and perspective of polymer white light-emitting devices and materials. *Chem. Soc. Rev.* **38**, 3391–3400 (2009).
20. Y. Zang, F. Zhang, D. Huang, X. Gao, C.-a. Di, D. Zhu, Flexible suspended gate organic thin-film transistors for ultra-sensitive pressure detection. *Nat. Commun.* **6**, 6269 (2015).
21. A. N. Sokolov, B. C.-K. Tee, C. J. Bettinger, J. B.-H. Tok, Z. Bao, Chemical and engineering approaches to enable organic field-effect transistors for electronic skin applications. *Acc. Chem. Res.* **45**, 361–371 (2012).
22. V. Coropceanu, J. Cornil, D. A. da Silva Filho, Y. Olivier, R. Silbey, J.-L. Brédas, Charge transport in organic semiconductors. *Chem. Rev.* **107**, 926–952 (2007).
23. J. L. Brédas, J. P. Calbert, D. A. da Silva Filho, J. Cornil, Organic semiconductors: A theoretical characterization of the basic parameters governing charge transport. *Proc. Natl. Acad. Sci. U.S.A.* **99**, 5804–5809 (2002).
24. Y. Zhao, Y. Guo, Y. Liu, 25th anniversary article: Recent advances in n-type and ambipolar organic field-effect transistors. *Adv. Mater.* **25**, 5372–5391 (2013).
25. Z. Liu, G. Zhang, Z. Cai, X. Chen, H. Luo, Y. Li, J. Wang, D. Zhang, New organic semiconductors with imide/amide-containing molecular systems. *Adv. Mater.* **26**, 6965–6977 (2014).

Downloaded from http://advances.sciencemag.org/ on June 26, 2019

26. G. Giri, E. Verploegen, S. C. B. Mannsfeld, S. Atahan-Evrenk, D. H. Kim, S. Y. Lee, H. A. Becerril, A. Aspuru-Guzik, M. F. Toney, Z. Bao, Tuning charge transport in solution-sheared organic semiconductors using lattice strain. *Nature* **480**, 504–508 (2011).
27. Y. Diao, B. C.-K. Tee, G. Giri, J. Xu, D. H. Kim, H. A. Becerril, R. M. Stoltenberg, T. H. Lee, G. Xue, S. C. B. Mannsfeld, Z. Bao, Solution coating of large-area organic semiconductor thin films with aligned single-crystalline domains. *Nat. Mater.* **12**, 665–671 (2013).
28. H.-R. Tseng, H. Phan, C. Luo, M. Wang, L. A. Perez, S. N. Patel, L. Ying, E. J. Kramer, T.-Q. Nguyen, G. C. Bazan, A. J. Heeger, High-mobility field-effect transistors fabricated with macroscopic aligned semiconducting polymers. *Adv. Mater.* **26**, 2993–2998 (2014).
29. C. Luo, A. K. K. Kyaw, L. A. Perez, S. Patel, M. Wang, B. Grimm, G. C. Bazan, E. J. Kramer, A. J. Heeger, General strategy for self-assembly of highly oriented nanocrystalline semiconducting polymers with high mobility. *Nano Lett.* **14**, 2764–2771 (2014).
30. H. Sirringhaus, 25th anniversary article: Organic field-effect transistors: The path beyond amorphous silicon. *Adv. Mater.* **26**, 1319–1335 (2014).
31. R. Noriega, J. Rivnay, K. Vandewal, F. P. V. Koch, N. Stingelin, P. Smith, M. F. Toney, A. Salleo, A general relationship between disorder, aggregation and charge transport in conjugated polymers. *Nat. Mater.* **12**, 1038–1044 (2013).
32. D. Venkateshvaran, M. Nikolka, A. Sadhanala, V. Lemaur, M. Zelazny, M. Kepa, M. Hurhangee, A. J. Kronemeijer, V. Pecunia, I. Nasrallah, I. Romanov, K. Broch, I. McCulloch, D. Emin, Y. Olivier, J. Cornil, D. Beljonne, H. Sirringhaus, Approaching disorder-free transport in high-mobility conjugated polymers. *Nature* **515**, 384–388 (2014).
33. C.-Z. Li, C.-C. Chueh, H.-L. Yip, F. Ding, X. Li, A. K.-Y. Jen, Solution-processible highly conducting fullerenes. *Adv. Mater.* **25**, 2457–2461 (2013).
34. B. D. Naab, S. Zhang, K. Vandewal, A. Salleo, S. Barlow, S. R. Marder, Z. Bao, Effective solution- and vacuum-processed n-doping by dimers of benzimidazoline radicals. *Adv. Mater.* **26**, 4268–4272 (2014).
35. P. Wei, T. Menke, B. D. Naab, K. Leo, M. Riede, Z. Bao, 2-(2-Methoxyphenyl)-1,3-dimethyl-1*H*-benzoimidazol-3-ium iodide as a new air-stable n-type dopant for vacuum-processed organic semiconductor thin films. *J. Am. Chem. Soc.* **134**, 3999–4002 (2012).
36. Y. Zhang, H. Zhou, J. Seifter, L. Ying, A. Mikhailovsky, A. J. Heeger, G. C. Bazan, T.-Q. Nguyen, Molecular doping enhances photoconductivity in polymer bulk heterojunction solar cells. *Adv. Mater.* **25**, 7038–7044 (2013).
37. B. D. Naab, S. Himmelberger, Y. Diao, K. Vandewal, P. Wei, B. Lussem, A. Salleo, Z. Bao, High mobility n-Type transistors based on solution-sheared doped 6,13-bis(triisopropylsilylethynyl)pentacene thin films. *Adv. Mater.* **25**, 4663–4667 (2013).
38. L. Ma, W. H. Lee, Y. D. Park, J. S. Kim, H. S. Lee, K. Cho, High performance polythiophene thin-film transistors doped with very small amounts of an electron acceptor. *Appl. Phys. Lett.* **92**, 063310 (2008).
39. A. Pivrikas, H. Neugebauer, N. S. Sariciftci, Influence of processing additives to nano-morphology and efficiency of bulk-heterojunction solar cells: A comparative review. *Sol. Energy* **85**, 1226–1237 (2011).
40. H.-C. Liao, C.-C. Ho, C.-Y. Chang, M.-H. Jao, S. B. Darling, W.-F. Su, Additives for morphology control in high-efficiency organic solar cells. *Mater. Today* **16**, 326–336 (2013).
41. Y. Zhang, D. Hanifi, E. Lim, S. Chourou, S. Alvarez, A. Pun, A. Hexemer, B. Ma, Y. Liu, Enhancing the performance of solution-processed n-type organic field-effect transistors by blending with molecular "aligners". *Adv. Mater.* **26**, 1223–1228 (2014).
42. J. Smith, W. Zhang, R. Sougrat, K. Zhao, R. Li, D. Cha, A. Amassian, M. Heeney, I. McCulloch, T. D. Anthopoulos, Solution-processed small molecule-polymer blend organic thin-film transistors with hole mobility greater than 5 cm^2/Vs. *Adv. Mater.* **24**, 2441–2446 (2012).
43. J. Cho, K. H. Cheon, H. Ahn, K. H. Park, S.-K. Kwon, Y.-H. Kim, D. S. Chung, High charge-carrier mobility of 2.5 cm^2 V^{-1} s^{-1} from a water-borne colloid of a polymeric semiconductor via smart surfactant engineering. *Adv. Mater.* **27**, 5587–5592 (2015).
44. R. Hamilton, J. Smith, S. Ogier, M. Heeney, J. E. Anthony, I. McCulloch, J. Veres, D. D. C. Bradley, T. D. Anthopoulos, High-performance polymer-small molecule blend organic transistors. *Adv. Mater.* **21**, 1166–1171 (2009).
45. M. S. Chen, O. P. Lee, J. R. Niskala, A. T. Yiu, C. J. Tassone, K. Schmidt, P. M. Beaujuge, S. S. Onishi, M. F. Toney, A. Zettl, J. M. J. Fréchet, Enhanced solid-state order and field-effect hole mobility through control of nanoscale polymer aggregation. *J. Am. Chem. Soc.* **135**, 19229–19236 (2013).
46. L. Qiu, J. A. Lim, X. Wang, W. H. Lee, M. Hwang, K. Cho, Versatile use of vertical-phase-separation-induced bilayer structures in organic thin-film transistors. *Adv. Mater.* **20**, 1141–1145 (2008).
47. N. D. Treat, J. A. N. Malik, O. Reid, L. Yu, C. G. Shuttle, G. Rumbles,C. J. Hawker, M. L. Chabinyc, P. Smith, N. Stingelin, Microstructure formation in molecular and polymer semiconductors assisted by nucleation agents. *Nat. Mater.* **12**, 628–633 (2013).
48. Z. Chen, M. J. Lee, R. S. Ashraf, Y. Gu, S. Albert-Seifried, M. M. Nielsen, B. Schroeder, T. D. Anthopoulos, M. Heeney, I. McCulloch, H. Sirringhaus, High-performance ambipolar diketopyrrolopyrrole-thieno[3,2-*b*]thiophene copolymer field-effect transistors with balanced hole and electron mobilities. *Adv. Mater.* **24**, 647–652 (2012).
49. J. Li, Y. Zhao, H. S. Tan, Y. Guo, C.-A. Di, G. Yu, Y. Liu, M. Lin, S. H. Lim, Y. Zhou, H. Su, B. S. Ong, A stable solution-processed polymer semiconductor with record high-mobility for printed transistors. *Sci. Rep.* **2**, 754 (2012).
50. H. Chen, Y. Guo, G. Yu, Y. Zhao, J. Zhang, D. Gao, H. Liu, Y. Liu, Highly π-extended copolymers with diketopyrrolopyrrole moieties for high-performance field-effect transistors. *Adv. Mater.* **24**, 4618–4622 (2012).
51. J. Lee, A.-R. Han, H. Yu, T. J. Shin, C. Yang, J. H. Oh, Boosting the ambipolar performance of solution-processable polymer semiconductors via hybrid side-chain engineering. *J. Am. Chem. Soc.* **135**, 9540–9547 (2013).
52. H. J. Snaith, M. Grätzel, Enhanced charge mobility in a molecular hole transporter via addition of redox inactive ionic dopant: Implication to dye-sensitized solar cells. *Appl. Phys. Lett.* **89**, 262114 (2006).
53. A. J. Kronemeijer, V. Pecunia, D. Venkateshvaran, M. Nikolka, A. Sadhanala, J. Moriarty, M. Szumilo, H. Sirringhaus, Two-dimensional carrier distribution in top-gate polymer field-effect transistors: Correlation between width of density of localized states and Urbach energy. *Adv. Mater.* **26**, 728–733 (2014).
54. X. Zhang, L. J. Richter, D. M. DeLongchamp, R. J. Kline, M. R. Hammond, I. McCulloch, M. Heeney, R. S. Ashraf, J. N. Smith, T. D. Anthopoulos, B. Schroeder, Y. H. Geerts, D. A. Fischer, M. F. Toney, Molecular packing of high-mobility diketo pyrrolo-pyrrole polymer semiconductors with branched alkyl side chains. *J. Am. Chem. Soc.* **133**, 15073–15084 (2011).
55. X. Zhang, H. Bronstein, A. J. Kronemeijer, J. Smith, Y. Kim, R. J. Kline, L. J. Richter, T. D. Anthopoulos, H. Sirringhaus, K. Song, M. Heeney, W. Zhang, I. McCulloch, D. M. DeLongchamp, Molecular origin of high field-effect mobility in an indacenodithiophene–benzothiadiazole copolymer, *Nat. Commun.* **4**, 2238 (2013).
56. E. Gann, A. T. Young, B. A. Collins, H. Yan, J. Nasiatka, H. A. Padmore, H. Ade, A. Hexemer, C. Wang, Soft x-ray scattering facility at the Advanced Light Source with real-time data processing and analysis. *Rev. Sci. Instrum.* **83**, 045110 (2012).

Acknowledgments: D.Z. would like to thank D.-B. Zhu (Institute of Chemistry Chinese Academy of Sciences) and C.-A. Di (Institute of Chemistry Chinese Academy of Sciences) for helpful discussions. **Funding:** This work was financially supported by the National Natural Science Foundation of China (21190032), the Strategic Priority Research Program of the Chinese Academy of Sciences (XDB12010300), and the 973 Program project of the Ministry of Science and Technology of China. **Author contributions:** D.Z., Z.L., and H.S. initiated the study and proposed the mechanism. H.L., C.Y., and Z.L. carried out the experiments and analyzed the data. G.Z., H.G., and Y.Y. carried out the ^{13}C NMR measurements and theoretical calculations. K.B., Y.H., A.S., and L.J. carried out the PDS and SKPM experiments. Z.C., P.Q., and Z.L. synthesized DPPTTT. D.Z., H.S., and Z.L. prepared the manuscript. All authors discussed, revised, and approved the manuscript. **Competing interests:** The authors declare that they have no competing interests. **Data and materials availability:** All data needed to evaluate the conclusions in the paper are present in the paper and/or the Supplementary Materials. Additional data related to this paper may be requested from the authors by emailing zitong_@iccas.ac.cn and dqzhang@iccas.ac.cn.

Submitted 16 January 2016
Accepted 14 April 2016
Published 13 May 2016
10.1126/sciadv.1600076

Citation: H. Luo, C. Yu, Z. Liu, G. Zhang, H. Geng, Y. Yi, K. Broch, Y. Hu, A. Sadhanala, L. Jiang, P. Qi, Z. Cai, H. Sirringhaus, D. Zhang, Remarkable enhancement of charge carrier mobility of conjugated polymer field-effect transistors upon incorporating an ionic additive. *Sci. Adv.* **2**, e1600076 (2016).

Downloaded from http://advances.sciencemag.org/ on June 26, 2019

Science Advances

Remarkable enhancement of charge carrier mobility of conjugated polymer field-effect transistors upon incorporating an ionic additive

Hewei Luo, Chenmin Yu, Zitong Liu, Guanxin Zhang, Hua Geng, Yuanping Yi, Katharina Broch, Yuanyuan Hu, Aditya Sadhanala, Lang Jiang, Penglin Qi, Zhengxu Cai, Henning Sirringhaus and Deqing Zhang

Sci Adv **2** (5), e1600076.
DOI: 10.1126/sciadv.1600076

ARTICLE TOOLS http://advances.sciencemag.org/content/2/5/e1600076

SUPPLEMENTARY MATERIALS http://advances.sciencemag.org/content/suppl/2016/05/10/2.5.e1600076.DC1

REFERENCES This article cites 55 articles, 3 of which you can access for free
http://advances.sciencemag.org/content/2/5/e1600076#BIBL

PERMISSIONS http://www.sciencemag.org/help/reprints-and-permissions

Use of this article is subject to the Terms of Service

Science Advances (ISSN 2375-2548) is published by the American Association for the Advancement of Science, 1200 New York Avenue NW, Washington, DC 20005. 2017 © The Authors, some rights reserved; exclusive licensee American Association for the Advancement of Science. No claim to original U.S. Government Works. The title *Science Advances* is a registered trademark of AAAS.

Downloaded from http://advances.sciencemag.org/ on June 26, 2019